Poly(vinyl alcohol) Nanocomposites with Sepiolite and Heat-Treated Sepiolites

M. Alkan,[1] R. Benlikaya[2]

[1]*Department of Chemistry, Balikesir University, Balikesir, Turkey*
[2]*Department of Secondary Science and Mathematics Education, Balikesir University, Balikesir, Turkey*

Received 3 December 2007; accepted 30 November 2008
DOI 10.1002/app.29830
Published online 12 March 2009 in Wiley InterScience (www.interscience.wiley.com).

ABSTRACT: Poly(vinyl alcohol) (PVA) nanocomposites with pristine sepiolite and heat-treated (HT) sepiolites were prepared by the method of solution dispersion. The measurements of XRD, FTIR, TEM, and AFM were used for the characterization of the nanocomposites. Furthermore, thermal and optical properties were investigated by TG/DTG/DTA and UV-visible transmission spectra, respectively. Both the effects of sepiolite/polymer ratio and the structural changes in sepiolite on heating were examined in terms of changes in the properties of the nanocomposites. The addition of sepiolite/HT sepiolites into the PVA matrix resulted in a decrease in the thermal decomposition temperatures of the nanocomposites because of the fact that sepiolite and HT sepiolites facilitated the elimination of the water and acetate groups from the PVA in the second step based on the TG/DTG studies. The HT sepiolites-PVA nanocomposites had lower thermal stability and more influenced optical clarity than those of the sepiolite PVA, at the same filler levels. © 2009 Wiley Periodicals, Inc. J Appl Polym Sci 112: 3764–3774, 2009

Key words: sepiolite-PVA; poly(vinyl alcohol); nanocomposites

INTRODUCTION

Polymer materials are usually filled with several synthetic and/or natural layered silicates to increase some properties like heat resistance, mechanical strength, and impact resistance or to decrease other properties such as electrical conductivity or permeability for gases like oxygen or water vapor.[1]

For the production of polymer nanocomposites, 1 : 1 type layered silicates; 2 : 1 type layered silicates, and layered silicic acids are used.[2] The 2 : 1 units in sepiolite used in this study are arranged as indicated in Figure 1. Sepiolite is a hydrous magnesium silicate with $(Si_{12}Mg_8O_{30})(OH)_4(OH_2)_4{\cdot}8H_2O$ as the theoretical unit cell formula. Each block is formed of an octahedral sheet of magnesium oxide/hydroxide packed between two tetrahedral silica layers. The blocks are not sheets but ribbons which are linked forming an open cavity (i.e., tunnel) similar to that of zeolites, in which water (zeolitic water) and exchange ions can be accommodated.[3] Each one of the Mg^{2+} cations located at the edges of the octahedral sheets (i.e., those with access to the tunnels) complete their octahedral coordination, for they are bound to two molecules of water (coordinated water). The external surface of sepiolite microfibers are composed of channels and structural steps, as determined by the external blocks' distribution.[4]

Sepiolite is also a good adsorbent for organic species because it exhibits a variety of attractive properties such as high specific surface area, porosity, and surface activity. Sepiolite is therefore used in a large spectrum of areas where its sorptive, catalytic, and rheological properties are exploited. Investigations on sepiolite have so far focused more on its sorptive properties.[5] A number of investigators have studied the interaction of water and various organic reagents with sepiolite.[5–11]

The papers related to heat-treated (HT) sepiolites are usually concentrated on adsorption.[9–11] Although the differences relating to the adsorption behaviors between sepiolite and HT sepiolites have been discussed, no study to date has appeared on sepiolite-polymer nanocomposites.

Considering the studies on the nanocomposites with sepiolite, it is seen that polyurethane,[12] poly (hydroxyethyl acrylate),[13] and poly(sodium acrylate)[14] for *in situ* polymerization method; chitosan,[15] epoxy resin,[16,17] poly(dimetylsiloxane),[18,19] poly (ethyl methacrylate), and poly(2-hydroxyethyl methacrylate)[20] for solution dispersion; Nylon-6,[21] polypropylene[22] for melt intercalation and polypropylene[23] for supercritical CO_2-assisted mixing have been used in the relevant experiments. Nanofibers of sepiolite have proved to yield substantial improvement for the mechanical properties[13,15,16,18,19] and thermal stability[12,15,17,20] of these polymers even at low filler levels.

Correspondence to: M. Alkan (malkan@balikesir.edu.tr).
Contract grant sponsor: Balikesir University; contract grant number: 2006/01.

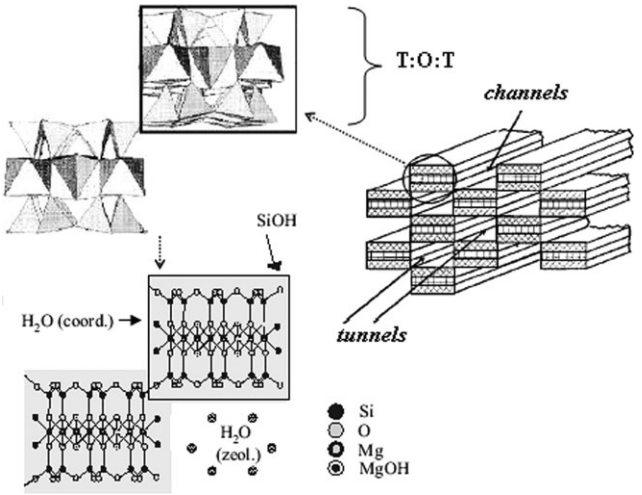

Figure 1 The structure of sepiolite.

Poly(vinyl alcohol) (PVA) is a water-soluble polymer extensively used in paper coating, textile sizing, flexible water-soluble packaging films, etc.[24] As both the sepiolite and PVA are very hydrophilic, sepiolite can be incorporated into PVA without need for pretreatment by simply dispersing the two components in water.[25] Nanocomposites of PVA such as MMT,[24–29] saponite,[24,30] MoO_3,[31] hydrated calcium aluminate ceramic,[32] layered double hydroxide,[33] vermiculite,[34] laponite,[35] etc. were synthesized using the solution dispersion method. Also, PVA nanocomposites with silica (SiO_2),[36] MMT,[37] kaolinite,[38] iron, cobalt, or nickel sulfides,[39] $CoFe_2O_4$,[40] and silver[41] were prepared via a novel self-assembled monolayer technique, *in situ* polymerization,[37–38] a hydrothermal process, *in situ* precipitation and oxidation, and *in situ* reduction of silver, respectively. The mechanical,[24,29,36,37] thermal,[27,28,31,35–38] optical,[27,30,37] and permeability (water, oxygen, and solute)[27,28,30,35] properties of the nanocomposites were studied.

As mentioned earlier, no study related to the PVA nanocomposites with sepiolite/HT sepiolites has been reported so far in the literature. In this study, the relevant nanocomposites were prepared by solution dispersion method. The measurements of FTIR, XRD, TEM, AFM, TG/DTG, and UV-visible transmission spectra were used for the characterization of the nanocomposite samples. Both the effects of sepiolite/polymer ratio and the structural changes in sepiolite on heating were examined in terms of changes in the properties of the composites.

EXPERIMENT

Materials and methods

Sepiolite (JCPDS 29-1492) having the chemical composition given in Table I was provided from Aktaş Lületaşı Corp., Eskişehir, Turkey. PVA (87–89% hydrolyzed, M_w = 85,000–146,000) was obtained commercially from a company named Aldrich (USA).

Serna et al.[42] noted that the temperature range of phase transitions is dependent on the experimental conditions, such as the heating rate or whether the sample was heated in air or vacuum. In this work, sepiolite (≤75 μm) was calcined at 400, 600, and 900°C for 2 h (10°C/min) in a furnace under an air atmosphere. These calcined sepiolites are identified as Sep400, Sep600, and Sep900, respectively.

The solution dispersion method is frequently successful in preparation of PVA/clay nanocomposite, as was described in literature.[43,44] The required amount of sepiolite was dispersed in distilled water for 2 h at room temperature using a magnetic stirrer. After ultrasonic treatment for 20 min, PVA was added. The samples were then heated at 80°C for 4 h to ensure that PVA was completely dissolved. Then they were stirred for a day at room temperature. Finally, films were cast in a closed oven at 40°C for 2 days. The film thicknesses were controlled by solution volume.

Characterization

FTIR experiments were performed with a Perkin–Elmer Spectrum One for scanning coverage from 650 to 4000 cm^{-1}. XRD patterns were obtained using Rigaku Rint 2000 diffractometer. The X-ray beam was derived from nickel-filtered Cu Kα (λ = 0.154 nm) radiation in a sealed tube operated at 40 kV, 30 mA, and the diffraction curves ranged from 5 to 50 at a scan rate of 0.02°/min. Atomic force microscopy was performed using a NanoMagnetics Instruments AFM[45] in tapping mode, using 300 kHz cantilevers having 40 N/m spring constant. Transmission electron microscopy was used to determine sepiolite's form (α or β) and morphology of PVA nanocomposites with sepiolite/HT sepiolites at an acceleration voltage of 100 kV. For TEM study the samples of PVA-sepiolite/HT sepiolites dispersions were deposited on a 200-mesh copper grid.

The thermal stability of the nanocomposites was examined using a Perkin–Elmer Pyris Diamond TG/

TABLE I
Chemical Composition of Sepiolite

Constituent	Percentage present
SiO_2	53.90
MgO	25.58
CaO	0.04
Al_2O_3	0.18
LoI	20.05

LoI, loss of ignition.

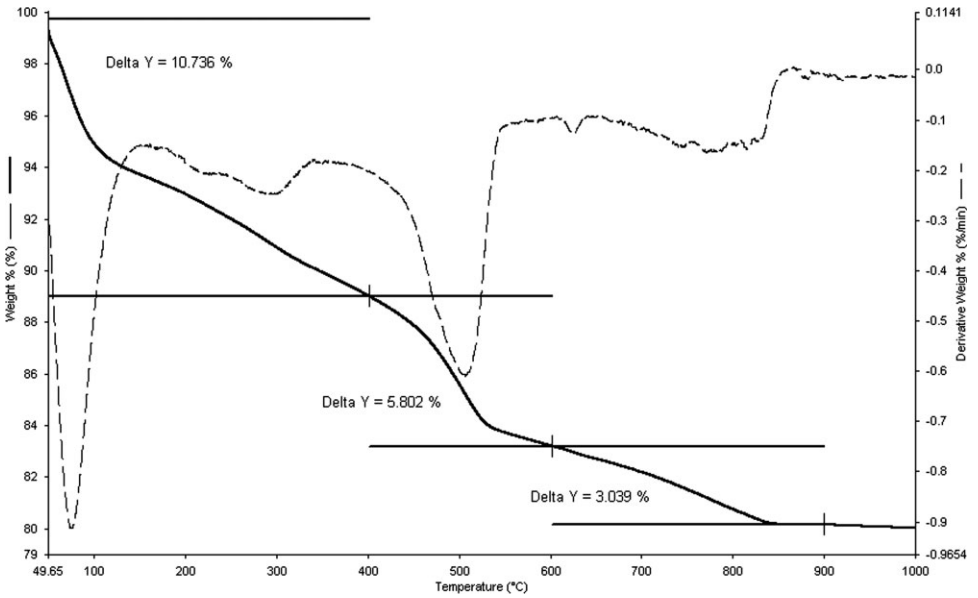

Figure 2 TG and DTG curves of sepiolite used in the study.

DTA. The TG scans were recorded at a temperature ramp of 10°C/min under a constant nitrogen flow of 200 mL/min from 50 to 600°C. While DTG curves were used to examine, if a change occurred in the thermal degradation mechanism of PVA, the T_m (melting-transition temperature) values of the composites were measured by DTA. Optical properties were investigated by Perkin–Elmer Lambda 25 UV visible spectrometer in the range of 190–1100 nm.

RESULTS AND DISCUSSION

Products of HT sepiolite

Numerous previous studies have monitored the dehydration of sepiolite using TGA and DTA methods.[46–49] Although the thermal properties of sepiolite have been the subject of many studies, calcined sepiolite samples were prepared to study the effect of heat treatment of sepiolite on PVA-sepiolite nanocomposite characteristics in this study. To determine the calcination temperatures, a TG study was carried out. To understand the effect of treatment, it would be useful to hold a brief discussion about the processes occurring during the calcination. According to our obtained TG data, Figure 2, the mass losses corresponding to three calcinations temperatures are assigned as follows:

- Up to 400°C, the loss of adsorbed water, zeolitic water, and the first water molecules coordinated to octahedral sheet (10.7%),
- From 400 to 600°C, the loss of the rest of the coordinated water molecules and dehydroxylation of the tetrahedral sheet (5.8%) and
- From 600 to 900°C, the loss of hydroxyl groups (3%).

Since the samples obtained at these temperatures were expected to behave differently from each other on the basis of the data obtained from TG of sepiolite, the sepiolite samples calcined at 400, 600, and 900°C were used in the study. In terms of the aforementioned findings, the reactions[48] occurring in heat treatments up to 1000°C can be summarized as

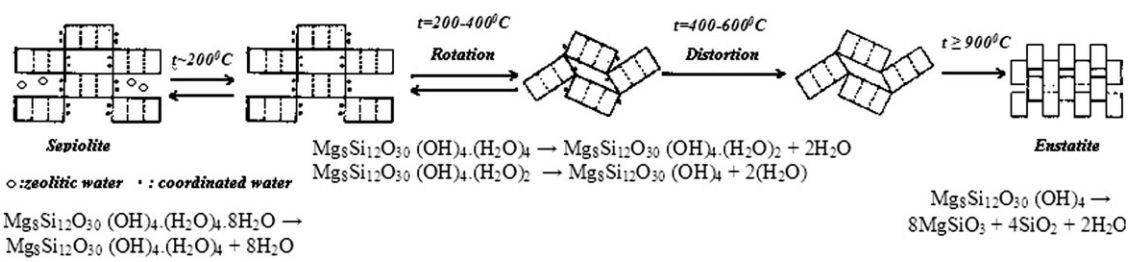

Figure 3 The summary of the reactions occurring during the heat activation of sepiolite.

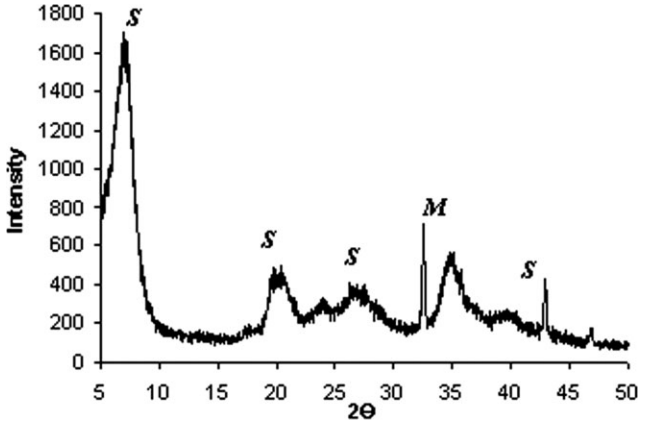

Figure 4 XRD pattern of sepiolite used in the study.

shown in Figure 3. As seen in the figure, sepiolite loses its water content and crystal structure changes during heating.

X-ray diffraction patterns of sepiolite and HT sepiolites

The XRD pattern of sepiolite used in this study shows the characteristic 110 peak of sepiolite at 1.23 nm and includes magnesite ($2\theta = 32.56°$, JCPDS 8-479) as the impurity in Figure 4. Furthermore, the TEM image of sepiolite in Figure 5 shows that it has a fibrous morphology.

The curves given in Figure 6 show that the intensity of the peak was reduced for heat activation products of sepiolite at 400 ($I \sim 1400$) and 600°C ($I \sim 1000$) due to the dehydration and structural folding of sepiolite. In addition, the peak related to magnesite between 30 and 35° disappeared at 600°C because of the removal of CO_2 from $MgCO_3$. When the peak at 1.23 nm was completely disappeared at 900°C, the peaks ($2\theta = 28°, 31°$) related to enstatite ($MgSiO_3$)[50] were observed. These findings confirm the reactions shown in Figure 4.

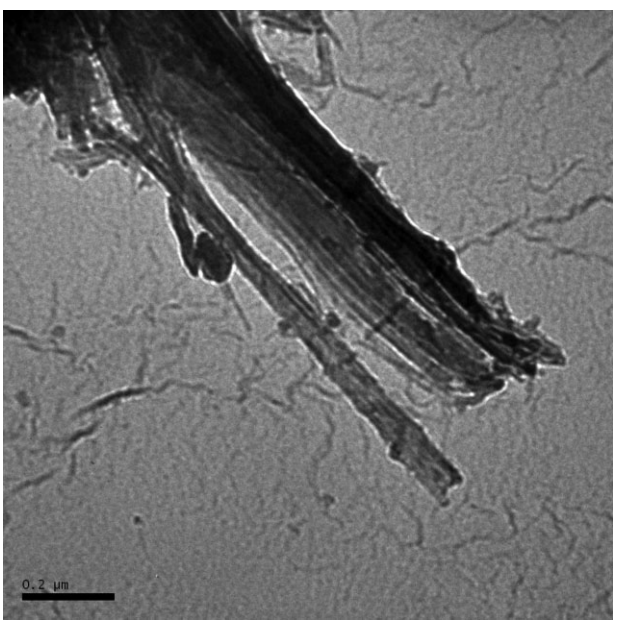

Figure 5 TEM image of sepiolite.

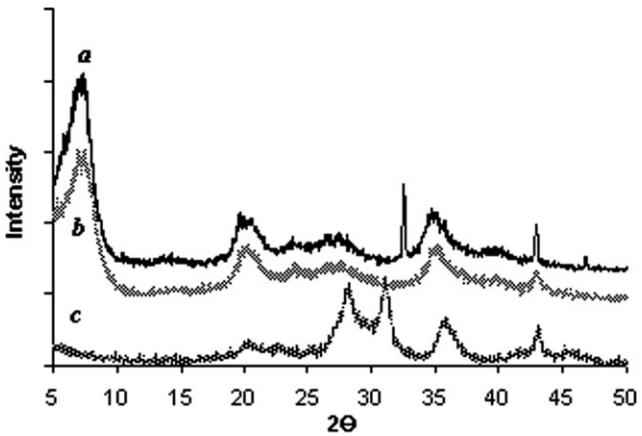

Figure 6 XRD patterns of HT sepiolite samples: Sep400 (a), Sep600 (b), and Sep900 (c).

FTIR spectra of sepiolite and HT sepiolites

Figure 7 shows FTIR spectra of pristine sepiolite, Sep400, Sep600, and Sep900. The heat-induced changes of peaks in regions of 4000–3000 cm^{-1} and 1700–1600 cm^{-1} are mainly due to the dehydration of zeolitic and bound water. While the bound water —OH bead at 1647 cm^{-1} shifted to 1618 and 1636 cm^{-1} in Sep 400 and Sep 600, respectively, this was not observed in Sep 900. The band related to CO_3^{-2} in sepiolite (1464 cm^{-1}) and Sep400 (1473 cm^{-1}) was not observed in Sep600 and Sep900. These data reach an agreement with XRD pattern of Sep600. The band of Si-O at 979 shifted to 1015 cm^{-1} (Sep400) and 1014 cm^{-1} (Sep600) on heating. The new bands ranging from 650 to 1100 cm^{-1} and

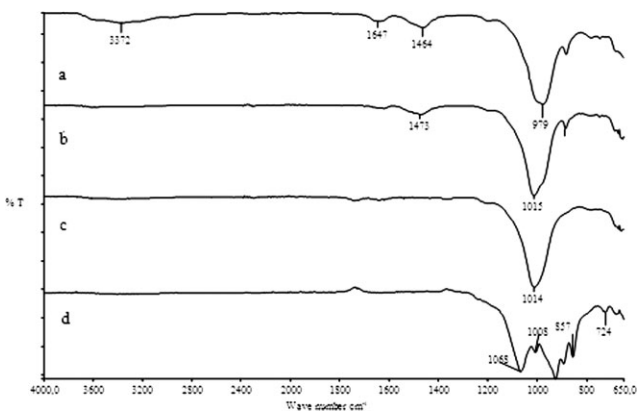

Figure 7 FTIR spectra of pristine and HT sepiolite samples: Sep400 (a), Sep600 (b), and Sep900 (c).

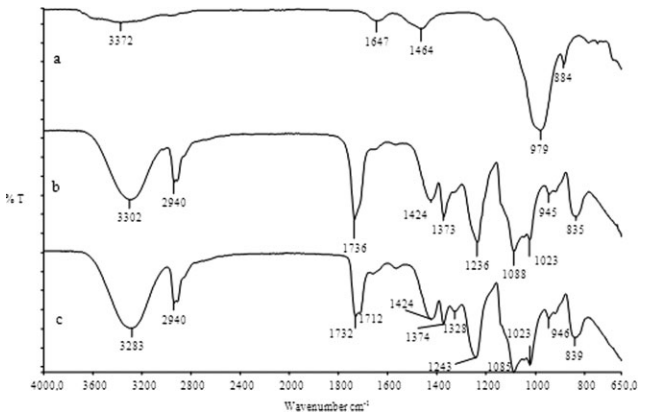

Figure 8 FTIR spectra of Sepiolite (a), PVA (b), and SepPVA1% (c).

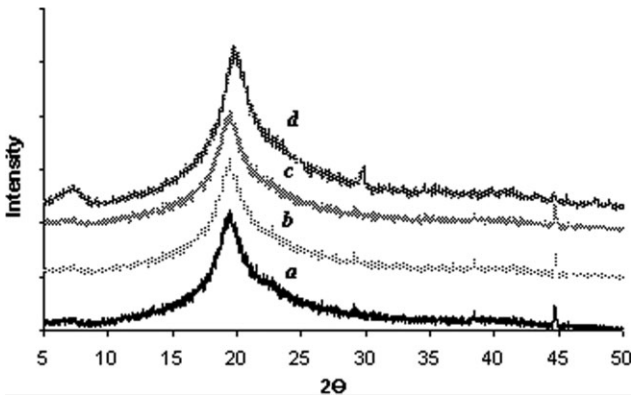

Figure 10 XRD patterns of PVA and sepiolite-PVA films: PVA (a), SepPVA1% (b), SepPVA2.5% (c), and SepPVA5% (d).

relating to enstatite[51] appeared in Sep900; confirm the phase transformation from sepiolite to enstatite in terms of reactions given in Figure 3.

FTIR spectra of the nanocomposites

The FTIR studies were carried out to understand the nature of any possible chemical and physical interactions between sepiolite/HT sepiolites and PVA. The FTIR spectrum of PVA in Figure 8 shows that the stretches of —CH_3, asymmetric —CH_2, and aliphatic —CH at 2940 and 2909 cm^{-1}, and C=O at 1736 cm^{-1} are most likely due to residual acetate groups still present in the partially hydrolyzed form of PVA. Furthermore, the spectrum of PVA film shows a band at 3302 cm^{-1} which was attributed to inter- and intramolecular hydrogen bonds in PVA. After the addition of sepiolite, the shift of the hydroxyl peak from 3302 to 3283 cm^{-1} arises from the strengthening of hydrogen bonds due to hydrogen bonding between silanol groups (—SiOH) on the surface of sepiolite and PVA. C=O stretching at 1736 cm^{-1} in PVA was shifted to 1732 and the band of C—O stretching shifted from 1088 to 1085 cm^{-1}. The hydrogen-bonded C=O bands at $\sim$ 1710 cm^{-1} were observed, in addition to the free C=O band for PVA-sepiolite/HT sepiolites composites. The new absorption bands at 2940 and 1732 cm^{-1}, appeared in the spectrum of Sep-PVA1% but not existing in pure sepiolite, were assigned to —CH_3 and C=O, respectively.

As for the PVA nanocomposites with HT sepiolites, the band of —OH at 3302 cm^{-1} in PVA were observed at 3301, 3288, and 3295 cm^{-1} for Sep400, Sep600, and Sep 900, respectively, as shown in Figure 9. While the hydrogen-bonded C=O band at $\sim$ 1710 cm^{-1} in Sep400PVA1% was the same as that of SepPVA1%, the band shifted to lower wave number in Sep600PVA1% and higher wave number in Sep900PVA1%. That the peak of aliphatic —CH_2 at

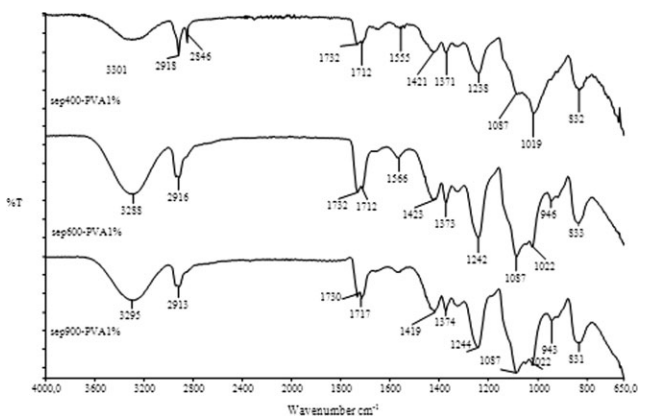

Figure 9 FTIR spectra of composites of PVA with HT sepiolites: PVA (a), Sep400PVA1% (b), Sep600PVA1% (c), and Sep900PVA1% (d).

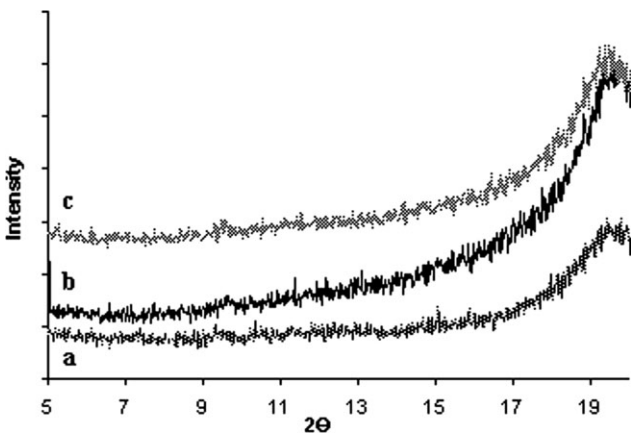

Figure 11 XRD patterns of HT sepiolite-PVA films: Sep400PVA1% (a), Sep600PVA1% (b), and Sep900PVA1% (c).

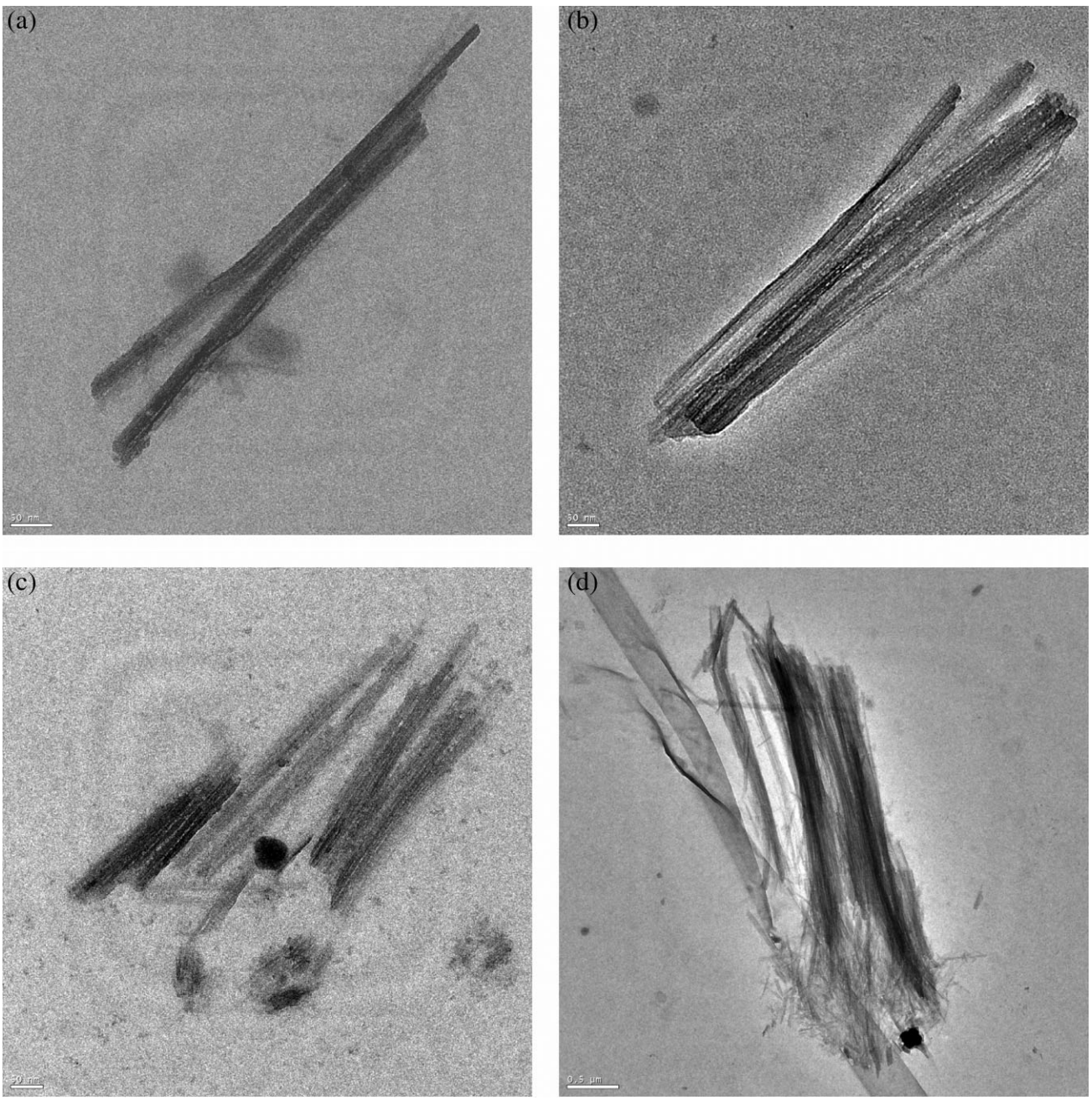

Figure 12 TEM images of the PVA nanocomposites: SepPVA1% (a, b) and Sep900PVA1% (c, d).

2909 cm^{-1} shifted to 2918 and 2913 cm^{-1} for HT sepiolites-PVA nanocomposites was an additional indication for interaction between HT sepiolites and PVA.

The above analysis indicated clearly that PVA matrix and sepiolite were not simply blended and some complex interactions existed. Their existence suggested that the structure of sepiolite surface was altered by the interactions with PVA as a result of some additional peaks and shifts in frequencies when compared with PVA. However, the similarity between the FTIR spectra taken from random locations of the nanocomposites was an indication of the fact that sepiolite had been dispersed uniformly in PVA matrix.

X-ray diffraction patterns of the nanocomposites

The XRD patterns for PVA and PVA nanocomposites with 1, 2.5, and 5 wt %, addition of sepiolite are shown in Figure 10. Sepiolite has normally a peak at $2\theta = 7.2^\circ$ (d: 1.23 nm). As shown in the figure, the disappearance of this basal peak for 1 and 2.5% of sepiolite-PVA nanocomposites is usually

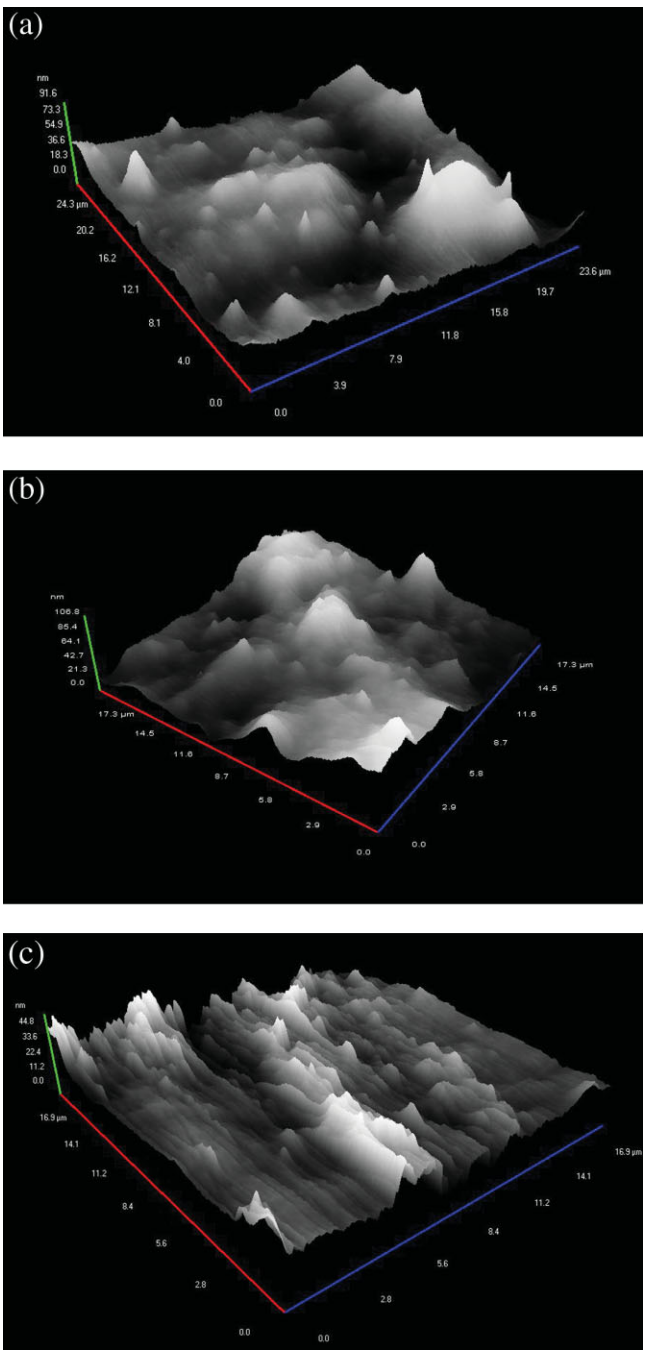

Figure 13 AFM images of sepiolite-PVA nanocomposites: SepPVA2.5% (a), SepPVA5% (b), Sep900VA5% (c). [Color figure can be viewed in the online issue, which is available at www.interscience.wiley.com.]

considered as an evidence for highly dispersion of sepiolite fibers. This change can be attributed to the fact that the texture in the sepiolite altered in the sepiolite-filled nanocomposites and then sepiolite is dispersed to fiber sticks or bundles and dispersed homogenously into PVA matrix. The intensity of 110 peak is related to the volume fraction of sepiolite fibers, i.e., the lower the volume fraction of the fibers, the more weak the diffraction peak.[12] For SepPVA5%, a relatively small diffraction peak displays at $2\theta = 7.2^\circ$. This is probably a consequence of the increase in the volume fraction compared with 1 and 2.5% and hence some sepiolite fibers agglomerate. The peak at $\sim 30^\circ$ 2θ is due to partially crystalline structure of PVA. Furthermore, the XRD patterns of Sep400PVA1%, Sep600PVA1%, and Sep900PVA1% in Figure 11 show that HT sepiolites are dispersed homogenously into PVA matrix by 1%.

TEM images of the nanocomposites

TEM images can give information about the morphology of nanocomposite. In this study, TEM images of SepPVA1% and Sep900PVA1% were obtained because XRD pattern of Sep900 had not included the 110 peak of sepiolite at $2\theta = 7.2^\circ$ as mentioned before (Fig. 6). In the TEM images of SepPVA1%, the fiber bundles with diameters which are not uniform in nanoscale were observed as can be seen in Figure 12(a,b). In that of Sep900PVA%1 [Fig. 12(c,d)], wider fiber bundles, presumably

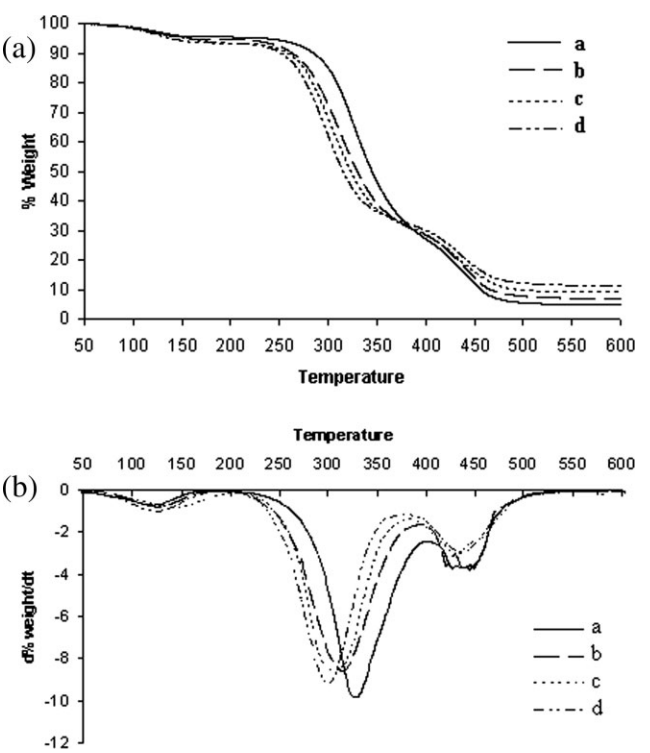

Figure 14 Thermogravimetric curves of sepiolite-PVA nanocomposites: (a) TG curves and (b) DTG curves, PVA (curve a), SepPVA1% (curve b), SepPVA2.5% (curve c), and SepPVA5% (curve d).

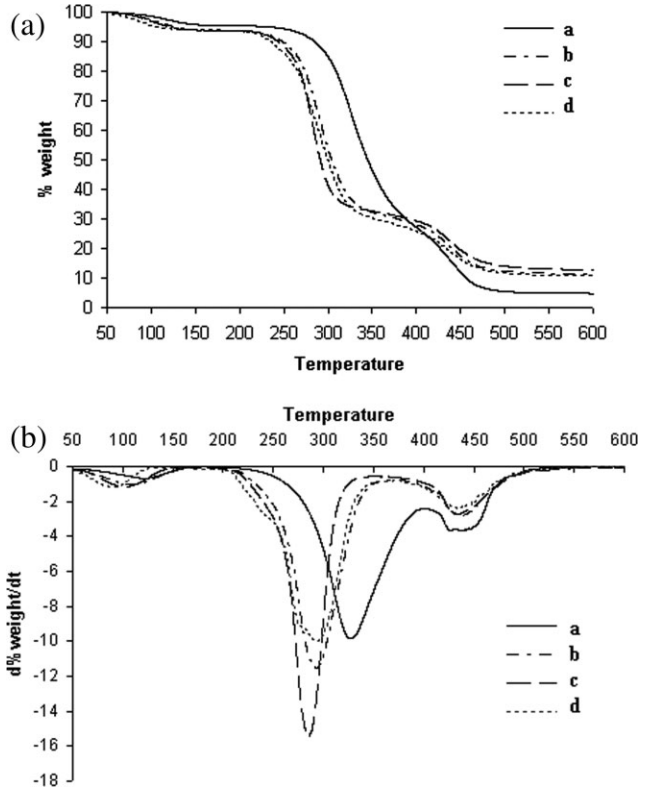

Figure 15 Thermogravimetric curves of HT sepiolite-PVA nanocomposites: (a) TG curves and (b) DTG curves, PVA (curve a), Sep400PVA5% (curve b), Sep600PVA5% (curve c), and Sep900PVA5% (d).

belonging to enstatite, compared with the fiber bundles of SepPVA1% were observed.

AFM images of the nanocomposites

Deneuborg et al.[18] observed that though some sepiolite needles were lying on the surface, most needles localized perpendicular to the surface in AFM analysis of polydimethylsiloxane-sepiolite nanocomposites. Therefore, 3D AFM morphology was used to observe the fibers perpendicular to the surface in the sepiolite-PVA nanocomposites as seen in Figure 13(a,b). The fibers appeared more evidently in Sep-PVA2.5% than Sep-PVA 5%. The increase in the volume fractions of the fibers was observed in 3D AFM morphology of Sep-PVA5% in comparison to Sep-PVA2.5%.

Figure 13c shows that the fiber bundles of sepiolite were observed in 3D morphology of SepPVA5%, they did not appear in that of Sep900PVA5% because all the sepiolite had been transformed into enstatite and the wider enstatite bundles caused the wider hills. All results regarding the AFM analysis were in agreement with the data obtained by XRD on the basis of the changes in volume fractions of sepiolite fibers.

Thermal properties of the nanocomposites

Figures 14 and 15 show the TG and DTG thermograms of PVA and its nanocomposites' films heated in a nitrogen atmosphere. The relevant data are summarized in Table II. According to these findings, the thermal degradation of PVA film and nanocomposites show three weight loss stages, as shown in the literature.[38,52] The reactions in these stages for PVA are shown in Figure 16. The first weight loss takes place at 50–176°C due to the loss of adsorbed moisture and/or evaporation of the trapped water; the second stage at 200–400°C involves the elimination reactions of H_2O and residual acetate groups because of partially hydrolyzed PVA. The degradation step at 400–550°C is more complex and includes the further degradation of polyene residues to yield the carbon and hydrocarbons[53] shown in Figure 16.

The reason for the weight loss in the first step may be caused by the evaporation of adsorbed moisture and/or trapped solvent due to the interactions among PVA, water/solvent, and sepiolite/HT sepiolites as shown in Figure 17 according to the data obtained by FTIR spectra and TG curves. The decrease in T_p (the temperature of the maximum weight loss rate) shows that sepiolite and HT sepiolites may facilitate the degradation of PVA in the second step. Furthermore, T_p temperatures for composites with HT sepiolites are lower than those with Sep-PVA. Generally speaking, thermal stability of the nanocomposites is lower than that of pure PVA. As previously mentioned this reduced thermal stability of sepiolite-PVA nanocomposites is presumably as a result of the reduction in the number of intra and inter hydrogen bonds of PVA after the addition of sepiolite/HT sepiolites. Additionally, they facilitate the removal of —OH and —$OOCCH_3$ groups.

As demonstrated in Table II, the char yield increased with the amount of sepiolite and HT sepiolites. This enhancement of the char formation

TABLE II
The Data Obtained from TG/DTG and DTA Curves for PVA and the Composites

Systems	T_m	T_p	% Char
PVA film	186	328	4.7
Sep-PVA1%	188	315	6.7
Sep-PVA2.5%	190	306	9.1
Sep-PVA5%	188	300	11.2
Sep400PVA1%	189	298	6.6
Sep400PVA5%	190	293	11.3
Sep600PVA1%	187	293	7.9
Sep600PVA5%	190	285	12.8
Sep900PVA1%	188	304	7.1
Sep900PVA5%	188	294	10.9

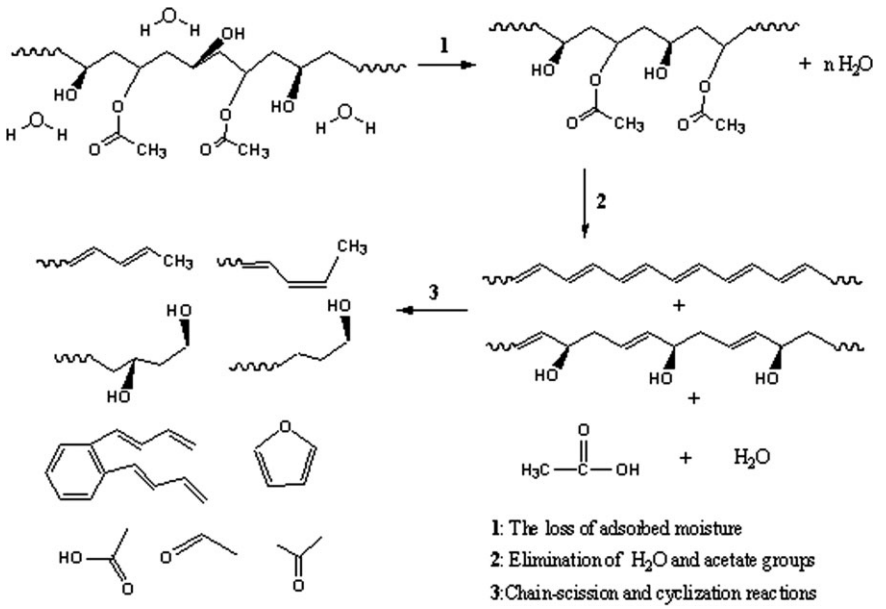

Figure 16 Reaction scheme occurring during the degradation of PVA.

was ascribed to the high heat resistance exerted by sepiolite and HT sepiolites.

The different types of fillers were found to have different influences on the thermal stability of PVA matrix. For example, while silver nanoparticles improve the thermal stability[54] of PVA, magnetite nanoparticles[55] and laponit[36] cause it to decrease. On the other hand, in the presence of montmorillonite in PVA as filler, the thermal decomposition remains unchanged.

The melting transition peaks of the PVA composites with various sepiolite/HT sepiolites loading were found to be slightly increased in the DTA curves, as is evident in Figure 18 and Table II. Similar results were obtained in the case of the montmorillonite/PVA nanocomposites[26] and the PbS/PVA nanocomposites[56] with low content of the inorganic phase.

Optical properties of the nanocomposites

The thickness of the films of bulk PVA and its composites used for optical property measurements is 50 ± 5 μm. Figure 18 shows UV-visible transmission spectra of PVA nanocomposites with sepiolite/HT sepiolites. The transmission spectra of PVA composites with sepiolite/HT sepiolites in 190–1100 nm are slightly affected by the presence of the low sepiolite loading. These products can be used in paper coatings, one of the most common uses for pure PVA. However, the spectra of the nanocomposites with HT sepiolites are more affected by filler loading and exhibit lower optical clarity than untreated sepiolite-PVA composites [Fig. 19(b–d)], suggesting that there

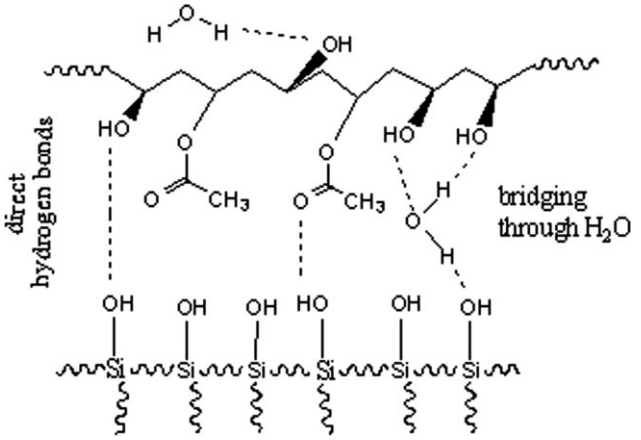

Figure 17 Interactions among PVA, water, and sepiolite.

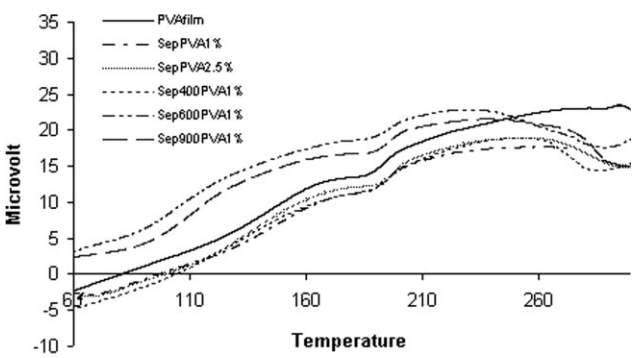

Figure 18 DTA curves of sepiolite-PVA nanocomposites: PVA (a), SepPVA1% (b), SepPVA2.5% (c), Sep400PVA1% (d), Sep600PVA1% (e), and Sep900PVA1% (f).

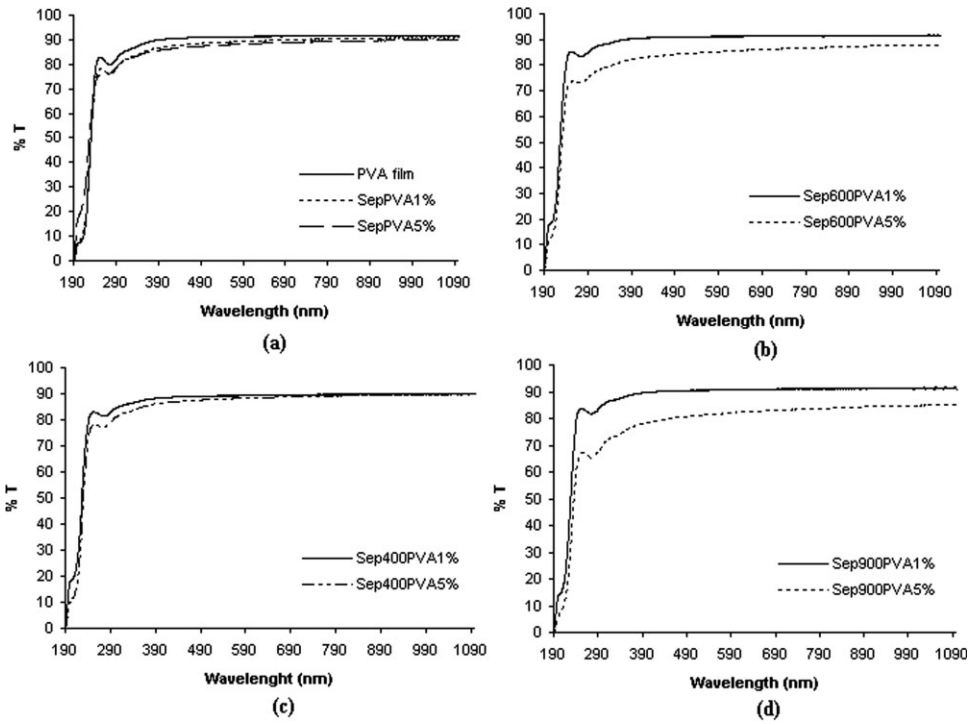

Figure 19 The effect of clay loading on optical properties of sepiolite/HT sepiolites-PVA films, Sepiolite (a), Sep400 (b), Sep600 (c), and Sep900 (d).

is stronger scattering of HT sepiolites resulting in lower transparency. This result is in agreement with the finding given in discussions of TEM images of Sep900PVA1%, in which enstatite formed by the bonding of fibers during the heating of sepiolite is used in the preparation of the nanocomposites.

CONCLUSIONS

The purpose of this study is to prepare PVA nanocomposites with sepiolite/HT sepiolites by the solution dispersion method and to investigate the influences of heat activation and loading percent of sepiolite on the properties and morphology of PVA nanocomposites. To investigate the effect of heat treatment of sepiolite on the properties of sepiolite-PVA nanocomposites, we used sepiolite samples heated at various temperatures such as 400, 600, and 900°C. The FTIR measurements showed that sepiolite fibers were dispersed inside the PVA matrix, causing the PVA to undergo significant changes on exfoliation with sepiolite. The XRD patterns, the AFM and the TEM images confirmed the dispersion of sepiolite fibers in the matrix.

The thermal properties of PVA and its' composites were investigated by TG, DTG, and DTA and the optical clarity by UV-visible transmission spectra. The addition of sepiolite/HT sepiolites into the PVA matrix resulted in a rise both in the char yield and in the melting temperatures; however, a decrease was observed in the thermal decomposition temperatures. These changes occurred due to the fact that sepiolite and HT sepiolites facilitated the elimination of water and acetate groups from PVA in the second step. Therefore, the heat treatment of sepiolite causes lower thermal stability and more influenced optical clarity when filler loading is added to the PVA.

The authors thank Prof. İsmet Kaya for FTIR measurements, Nanomagnetics Instrument for AFM analysis, and UNAM for TEM analysis.

References

1. Fischer, H. Mater Sci Eng C 2003, 23, 763.
2. Zeng, Q. H.; Yu, A. B.; Lu, G. Q.; Paul, D. R. J Nanosci Nanotech 2005, 5, 1574.
3. Velde B. Introduction to Clay Minerals: Chemistry, Origins, Uses and Environmental Significance; Chapman & Hall, 1992.
4. Fernandez-Saavedra, R.; Aranda, P.; Ruiz-Hitzky, E. Adv Funct Mater 2004, 14, 77.
5. Alkan, M.; Tekin, G.; Namli, H. Micro Meso Mater 2005, 84, 75.
6. Balci, S.; Dincel, Y. Chem Eng Process 2002, 41, 79.
7. Rytwo, R.; Nir, S.; Crespin, M.; Margulies, L. J Colloid Interface Sci 2000, 222, 12.
8. Gonzales-Pradas, E.; Valverda-Garcia, A.; Villafrance-Sanchez, M. J Chem Technol Biotechnol 1990, 47, 15.
9. González-Pradas, E.; Socías-Viciana, M.; Ureña-Amate, M. D.; Cantos-Molina, A.; Villafranca-Sánchez, M. Water Res 2005, 39, 1849.
10. Sabah, E.; Turan, M.; Çelik, M. S. Water Res 2002, 36, 3957.
11. Alkan, M.; Demirbaş, Ö.; Çelikçapa, S.; Doğan, M. J Hazard Mater 2004, 116, 135.
12. Chen, H.; Zheng, M.; Suna, H.; Jia, O. Mater Sci Eng A 2007, 15, 725.

13. Bokobza, L.; Burr, A.; Garnaud, G.; Perin, M. Y.; Pagnotta, S. Polym Int 2004, 53, 1060.
14. Santiago, F.; Mucientes, A. E.; Osorio, M.; Poblete, F. J. Polym Int 2006, 55, 843.
15. Darder, M.; Lopez-Blanco, M.; Aranda, P.; Aznar, A. J.; Bravo, J.; Ruiz-Hitzky, E. Chem Mater 2006, 18, 1602.
16. Zheng, Y.; Zheng, Y. J Appl Polym Sci 2006, 99, 2163.
17. Toldy, A.; Toth, N.; Keglevich, Gy.; Kiss, K.; Marosi, Gy. Polym Adv Technol 2006, 17, 778.
18. Deneuborg, F.-X.; Beigbeder, A.; Degee, Ph.; Viville, P.; Dubois, Ph. Silicone-Based Nanocomposites: New Materials for Antifouling Coatings. Available at: http://morris.umh.ac.be/SMPC/Posters/2006-BPG-FRDE.pdf (accessed June 2007).
19. Bokobza, L. J Appl Polym Sci 2004, 93, 2095.
20. Benlikaya, R.; Alkan, M.; Kaya, İ. Polym Compos, to appear.
21. Xie, S.; Zhang, S.; Wang, F.; Yang, M.; Séguéla, R.; Lefebvre, J.-M. Compos Sci Technol 2007, 67, 2334.
22. Ma, J.; Bilotti, E.; Peijs, T.; Darr, J. A. Eur Polym Sci 2007, 43, 4931.
23. Bilotti, E.; Fischer, H. R.; Peijs, T. J Appl Polym Sci 2008, 107, 116.
24. Chang, J.-H.; Jang, T.-G.; Ihn, K. J.; Lee, W.-K.; Sur, G. S. J Appl Polym Sci 2003, 90, 3208.
25. Döppers, L.-M.; Bren, C.; Sammon, C. Vib Spectrosc 2004, 35, 27.
26. Strawhecker, K. E.; Manias, E. Chem Mater 2000, 12, 2943.
27. Yeh, J.-M.; Ming-Yao, Y.; Shir-Joe, L. J Appl Polym Sci 2003, 89, 3632.
28. Strawhecker, K. E.; Manias, E. Macromolecules 2001, 34, 8475.
29. Wang, L.-P.; Wang, Y.-P.; Zhang, F.-A. Polym Compos 2005, 13, 839.
30. Yeun, J.-H.; Bang, G.-K.; Park, B. J.; Ham, S. K.; Chang, J.-H. J Appl Polym Sci 2006, 101, 591.
31. Lagashetty, A.; Havanoor, V.; Basavaraja, S.; Venkataraman, A. Bull Mater Sci 2005, 28, 477.
32. Messermith, P. B.; Osenar, P.; Stupp, S. I. J Mater Res 1999, 14, 315.
33. Li, B.; Hu, Y.; Zhang, R.; Chen, Z.; Fan, W. Mater Res Bull 2003, 38, 1567.
34. Xu, J.; Meng, Y. Z.; Li, R. K. Y.; Xu, Y.; Rajulu, A. V. J Polym Sci Part B: Polym Phys 2003, 41, 749.
35. Nair, S. H.; Pawar, K. C.; Jog, J. P.; Badiger, M. V. J Appl Polym Sci 2006, 103, 2896.
36. Zheng, P.; Kong, L. X.; Li, S.-D. J Appl Polym Sci 2005, 96, 1436.
37. Yu, Y.-H.; Lin, C.-Y.; Yeh, J.-M.; Lin, W.-H. Polymer 2003, 44, 3553.
38. Jia, X.; Li, Y.; Zhang, B.; Cheng, Q.; Zhang, S., Mat Res Bull 2008, 44, 611.
39. Qıan, X. F.; Yın, J.; Yang, Y. F.; Lu, Q. H.; Zhu, Z. K.; Lu, J. J Appl Polym Sci 2001, 82, 2744.
40. LóPez, D.; Cendoya, I.; Torres, F.; Tejada, J.; Mıjangos, C. J Appl Polym Sci 2001, 82, 3215.
41. Khanna, P. K.; Narendra, S.; Charan, S.; Subbarao V. V. V. S.; Gokhale, R.; Mulik, U. P. Mater Chem Phys 2005, 92, 229.
42. Serna, C.; Ahlrich, J. L.; Serratosa, J. M. Clays Clay Miner 1975, 23, 411.
43. Chiellini, E.; Corti, A.; D'Antone, S.; Solaro, R. Prog Polym Sci 2003, 28, 963.
44. Kaczmarek, H.; Podgorski, A. J Photochem Photobiol A 2007, 191, 209.
45. NanoMagnetics Instruments AFM. Available at: www.nanomagnetics-inst.com (accessed September 2008).
46. Ruiz, R.; del Moral, C.; Pesquera, C.; Benito, I.; Gonzalez, F. Thermochim Acta 1996, 279, 103.
47. Steudel, A.; Friedrich, F.; Weidler, P. G.; Nüesch, R.; Emmerich, K. DTTG 2006, 12, 50.
48. Nagata, H.; Shimoda, S.; Sudo, T. Clays Clay Miner 1974, 22, 285.
49. Post, J. E.; Bish, D. L.; Heaney, P. J. Am Mineral 2007, 92, 91.
50. Hernández, Y.; Carriazo J. G.; Almanza, O. Mater Charact 2006, 57, 44.
51. Kalinkina, E. V.; Kalinkin, A. M.; Forsling, W.; Makarov, V. N. Int J Miner Process 2001, 61, 289.
52. Goiti, E.; Salinas, M. M.; Arias, G.; Puglia, D.; Kenny, J. M.; Mijangos, C. Polym Degrad Stab 2007, 92, 2198.
53. Peng, Z.; Kong, L. X. Polym Degrad Stab 2007, 92, 1061.
54. Mbhele, Z. H.; Salemane, M. G.; van Sittert, C. G. C. E.; Nedeljković, J. M.; Djoković, V.; Luyt, A. S. Chem Mater 2003, 15, 5019.
55. Kumar, R. V.; Koltypin, Y.; Cohen, Y. S.; Aurbach, D.; Palchik, O.; Felner, I.; Gedanken, A. J. Mater Chem 2000, 10, 1125.
56. Kuljanin, J.; Ćomor, M. I.; Djoković, J. M.; Nedeljković, J. M. Mater Chem Phys 2006, 95, 67.